Journal of Materials Chemistry B

ROYAL SOCIETY OF CHEMISTRY

PAPER

View Article Online
View Journal

Cite this: DOI: 10.1039/d2tb00037g

Layered supramolecular hydrogels from thioglycosides†

Yu-Cheng Wang,[a] Laurel L. Kegel,‡[a] David S. Knoff,[b] Bhushan S. Deodhar,[a] Andrei V. Astashkin,[a] Minkyu Kim[bcd] and Jeanne E. Pemberton*[a]

Received 6th January 2022,
Accepted 13th April 2022

DOI: 10.1039/d2tb00037g

rsc.li/materials-b

Low molecular weight hydrogels are made of small molecules that aggregate *via* noncovalent interactions. Here, comprehensive characterization of the physical and chemical properties of hydrogels made from thioglycolipids of the disaccharides lactose and cellobiose with simple alkyl chains is reported. While thiolactoside hydrogels are robust, thiocellobioside gels are metastable, precipitating over time into fibrous crystals that can be entangled to create pseudo-hydrogels. Rheology confirms the viscoelastic solid nature of these hydrogels with storage moduli ranging from 10–600 kPa. Additionally, thiolactoside hydrogels are thixotropic which is a desirable property for many potential applications. Freeze-fracture electron microscopy of xerogels shows layers of stacked sheets that are entangled into networks. These structures are unique compared to the fibers or ribbons typically reported for hydrogels. Differential scanning calorimetry provides gel-to-liquid phase transition temperatures ranging from 30 to 80 °C. Prodan fluorescence spectroscopy allows assignment of phase transitions in the gels and other lyotropic phases of high concentration samples. Phase diagrams are estimated for all hydrogels at 1–10 wt% from 5 to ≥ 80 °C. These hydrogels represent a series of interesting materials with unique properties that make them attractive for numerous potential applications.

Introduction

Gels are unique materials made of molecules that assemble into a three-dimensional (3D) network with relevant spatial dimensions on the nanometer to micrometer range and immobilize solvent. Macroscopically, gels are viscoelastic solid materials. Depending on the nature of the interactions that hold together the 3D network of such gels, they can be classified as either chemical gels or physical gels. Chemical gels are made of molecules connected by covalent bonding and form a network of crosslinked polymer chains. In contrast, physical gels, sometimes referred to as supramolecular gels, are made of 3D networks held together by noncovalent interactions such as van der Waals interactions, the hydrophobic effect, π–π interactions, and hydrogen bonding. Chemical gels are generally thought to be more stable, with stronger mechanical properties than physical gels given the stronger interaction between monomers. However, over the past two decades, interest in physical gels has increased, as they are considered alternatives to chemical gels with the added advantages of being reversible between gel and sol, responsive to various stimuli, and more biocompatible and biodegradable, making them suitable for novel applications.[1]

Low molecular weight gels (LMWG), as a class of physical gels, are composed of small molecules that aggregate *via* noncovalent interactions; these generally form fibrous 3D networks that immobilize solvent.[2,3] LMWGs are generally known to be thermoreversible, gel at low concentration, and have high tolerance towards salts.[4,5] Given these unique properties, they have great potential for diverse applications in soft materials and biomaterials including catalysis, drug delivery, tissue engineering, nanoelectronics, environmental remediation, cosmetics, food and agricultural industry, and sensing.[2,6] Much effort has focused on the design of small molecules that can serve as low molecular weight hydrogelators as well as on improving their physicochemical properties for various applications.[7] The gelation behavior and mechanical properties

[a] Department of Chemistry and Biochemistry, University of Arizona, 1306 E University Boulevard, Tucson, Arizona 85721, USA. E-mail: pembertn@email.arizona.edu
[b] Department of Biomedical Engineering, University of Arizona, 1127 E James E Rogers Way, Tucson, AZ 85721, USA
[c] Department of Materials Science and Engineering, University of Arizona, 1235 E James E Rogers Way, Tucson, AZ 85721, USA
[d] BIO5 Institute, University of Arizona, 1657 E Helen Street, Tucson, AZ 85721, USA

† Electronic supplementary information (ESI) available: ^{1}H NMR, ^{13}C NMR, and mass spectrometric data for all compounds studied, additional rheology results, fluorescence spectra, powder X-ray diffraction data, and single crystal X-ray crystallography data. CCDC 2103128 and 2103513. For ESI and crystallographic data in CIF or other electronic format see DOI: https://doi.org/10.1039/d2tb00037g

‡ Current address: Bachem Americas, Inc., 3132 Kashiwa St, Torrance, CA 90505, USA.

of hydrogels are difficult to predict given the complex processes of self-assembly and 3D network formation, although approaches to tune properties such as mechanical properties have been reported.[3,8–11] Among all LMWGs, sugar–based gelators have gained special interest for use in novel soft materials due to their biodegradability and biocompatibility, as well as for their sourcing from renewable raw materials.[1,12,13] Sugar-based LMWGs have demonstrated their potential for use in many areas, including neural cell cultures,[14] scaffold for stem cells,[15] cell responsive capsules,[16] ionogel as electrolyte for electrochemical cells,[17,18] mercury ion sensor,[19] water purification,[20] gel electrophoresis,[21] optical devices,[22] although this work is still in its infancy and optimization of systems and properties is required.

Gelation properties of monosaccharide-based glycosylated amphiphiles,[23–34] disaccharide-based glycosylated amphiphiles,[32,35–39] bipolar glycosylated amphiphiles,[15,40] and open forms of sugar-based amphiphiles[30,41–44] with water and alcohol have been reported. These latter hydrogels have critical gelation concentrations in mixtures of alcohol and water or in pure aqueous solutions that range from 0.1 to 1 wt%, with fibrous hydrogel networks observed by electron microscopy. However, information about the thermal stability and rheological properties of these gels is relatively limited.

Clemente *et al.* have reported disaccharide-based hydrogelators made of lactose, cellobiose, and maltose with a triazole linkage through an amide bond to an alkyl chain with 16 carbons.[45] They showed that lactose and cellobiose, with a small stereochemical difference in the structure of the sugar moiety (axial or equatorial orientation of a single hydroxyl group), give rise to different molecular conformations within a network of twisted ribbons. Additionally, Yamanaka and coworkers synthesized urea-lactose/maltose-based hydrogels and demonstrated their potential use in drug delivery.[46–48]

In contrast, *S*-linked glycosylated amphiphiles, or thioglycolipids, have been reported only infrequently.[34,49–53] In our previous work, we reported initial observations of gelation with disaccharide based-thioglycolipids.[49] Five of the series of six thioglycolipid compounds reported here (Fig. 1) having either lactose (Lac) or cellobiose (Cel) head groups with varying alkyl chain lengths (C8, C10, C12) and β-S-glycosidic bonds (LacSC8, LacSC10, LacSC12 or CelSC10, CelSC12) form gels of varying stability and structure. As elaborated here in greater detail, not only do these gels have somewhat unusual properties relative to other sugar-based gels, the hydrogelator molecules from which they are made are quite easy and straightforward to synthesize with high efficiency at low cost relative to most of the sugar-based gel systems noted above. Here, we provide comprehensive characterization of these materials to unveil their physicochemical properties as a foundation for their use in applications. Different phases of the thioglycolipids at different concentrations were assessed by their visual appearance at different temperatures, mechanical properties by rheology at different temperatures, micro- and nano-structure by scanning electron microscopy (SEM) and transmission electron microscopy (TEM) on xerogels resulting from flash freezing and lyophilization of the hydrogels, phase transition temperatures by differential scanning calorimetry (DSC), and lyotropic phase microstructure by fluorescence spectroscopy at different temperatures using prodan, a polarity-sensitive dye. The collective whole of these results allowed phase diagrams for each thioglycolipid to be estimated. Different from most LMW hydrogels, these thiolactose-based hydrogels form disordered bicontinuous cubic 3D networks of lamellar bilayers, instead of the more commonly encountered fibrils or ribbons, with storage moduli (G') $>10^5$ Pa without optimization. Robust formation of these unique hydrogel microstructures could potentially be useful as materials with tunable G' values across broader range that might be important for applications such as 3D cell scaffolds,[54–56] biolubrication,[57,58] intelligent actuators,[59,60] superabsorbents,[61] and agriculture and food chemistry.[62,63] The green and high-yield synthetic process of the thioglycolipids, unique sulfur linkage between sugar and lipid moieties, sugar effect on the hydrogelation process, high storage modulus (G'), and unusual microstructure of these materials make them extremely unique and intriguing.

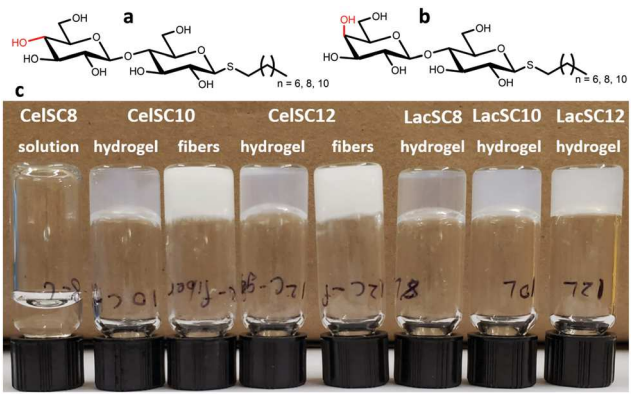

Fig. 1 Molecular structures of (a) alkyl-β-thiocellobiosides and (b) alkyl-β-thiolactobiosides, and (c) photographs of CelSC8 solution and gel formation for CelSC10, CelSC12, LacSC8, LacSC10, and LacSC12.

Experimental section

Synthetic procedures

Materials. Thiolactosides (LacSC*x* (x = 8, 10, 12) and thiocellobiosides (CelSC*x* (x = 8, 10, 12) were straightforwardly synthesized *via* a modified version of the methodology reported previously by Szabó *et al.*[64] Detailed synthesis procedures are described in the ESI† along with supporting spectral data (Fig S1–S18).

Preparation of hydrogels. Aqueous solutions of thioglycolipids were prepared by weighing 2–3 mg of thioglycolipid in 2 mL glass vials and adding an appropriate volume of water to make samples at desired concentrations. The vials were capped, sealed with Parafilm, heated to 75 °C (or 85 °C for LacSC12) until the thioglycolipids were completely dissolved (typically ~1 min) as indicated by the complete absence of turbidity. For LacSC*x* hydrogels, the samples were allowed to cool to ambient

temperature; during this cooling, hydrogels spontaneously form in under a minute once the solution reaches its transition temperature. Gels were allowed to equilibrate at room temperature for 15 min prior to analysis. For CelSC*x* hydrogels, samples were quenched at −4 °C in an ice/water bath and allowed to equilibrate at −4 °C for 15 min prior to analysis.

A similar protocol as just described was used to prepare hydrogels containing the fluorescent dye prodan. For these materials, water was replaced by an aqueous solution of 5 μM prodan (Molecular Probes) which was made by adding the appropriate amount of a prodan/ethanol stock solution to pure water, after which the ethanol was evaporated under vacuum.

Hydrogel characterization

Rheology. The viscoelastic mechanical properties of hydrogels were characterized using small amplitude oscillatory shear rheology on a Discovery Hybrid Rheometer 2 (TA Instruments, USA) in a cone-and-plate geometry consisting of a sandblasted 20 mm 1° cone and a sandblasted stage. Inertia, friction, and rotational mapping calibrations were performed prior to each experiment. A Peltier temperature-controlled stage maintained at 4, 10, 25, or 37 °C was used for all rheology testing. To ensure hydrogels are transferred without damage, hydrogels were made on the sample stage of the rheometer using the following procedure. First, hydrogel/water solutions were heated in a water bath to temperatures above their transition temperature for 5 min, then transferred to the sample stage as a viscous liquid before the cone portion of the sample stage was rapidly lowered (1–3 s) to the testing gap height of 50 μm. Excess gel was then trimmed from the edges of the geometry. To control evaporation, the geometry was encased in a solvent trap with a water seal and a mineral oil barrier was placed around the edges of the geometry. The temperature of the sample stage was maintained above the transition temperature for 15 min, then cooled for 15 min to either 25 or −4 °C depending on the thioglycolipid to allow formation of hydrogel. After this, the sample stage temperature was adjusted to the appropriate measurement temperature and the sample was equilibrated for 1 h prior to experimentation. Strain sweeps were performed from 0.01 to 1000% shear strain at a constant 10 rad s^{-1} angular frequency. G' and G'' values reported were determined by averaging the data points within the linear viscoelastic region of the strain sweep. Frequency sweeps were performed from 0.01 to 100 rad s^{-1} at a constant 0.01% shear strain. Thixotropy experiments were conducted by cycling the shear strain between 0.01% and 100%.

Electron microscopy. Scanning electron microscopy (SEM) was performed on an FEI Inspect S microscope equipped with a tungsten filament; standard secondary electron imaging was used. Xerogel samples of the hydrogels were prepared as follows. Hydrogels were first heated to the sol state and then pipetted onto an SEM-compatible sample stub. For LacSC*x* hydrogels and fibrous CelSC*x* samples, sample stubs were cooled to room temperature for 15 min to form hydrogels. For CelSC*x* hydrogels, sample stubs were quenched at −4 °C in an ice/water bath for 15 min to form hydrogels. The hydrogels so formed were then flash-frozen by immersion in liquid N_2 followed by lyophilization for 24 h in a VirTis Lyo-Centre 3.5L DBT benchtop lyophilizer. Samples were Au-coated before SEM characterization to reduce sample charging.

Transmission electron microscopy (TEM) was performed on a Hitachi HF-5000 to provide insight into the nanostructure of xerogels made from these thioglycolipids. To ensure films thin enough for TEM, xerogel preparation was as follows: lyophilization was performed immediately after hydrogel formation in a 1-dram vial. After lyophilization, hexane, a solvent in which the thioglycolipids are poorly soluble, was added to the vial followed by sonication for several sec. Then, 1 μL of the resulting solution was pipetted onto a carbon TEM grid (SPI Supplies Holey Carbon Coated Grids onto 100 Mesh Gold 3 mm). The grid was allowed to dry overnight before TEM imaging, during which time the hexane slowly evaporated.

Differential scanning calorimetry. A Mettler Toledo DSC 823e differential scanning calorimeter equipped with cooling apparatus was used for measurement of phase transition temperatures and enthalpies of the hydrogels. Samples were first made as described above and were then melted by heating to 75 °C (or 85 °C for LacSC12). Once completely in the sol state, small aliquots equating to ∼6 to 8 mg of material were pipetted into 40 μL aluminum DSC pans (DSC Consumables, Inc.) and capped with lids. The pans were maintained at 75 °C (or 85 °C) for 1 min to ensure sample melting. Then, the pans were cooled to and maintained at 5 °C for 20 min to ensure hydrogel formation. DSC data were then acquired for hydrogel samples heated from 5 to 85 °C at 5 °C min^{-1}.

Fluorescence spectroscopy. Steady-state fluorescence spectroscopy was performed on a Photon Technologies, Inc. Quanta Master 40 spectrofluorometer. Prodan fluorescence was excited at 350 nm with emission observed from 370 to 640 nm. LacSC8, LacSC10, LacSC12, CelSC8, CelSC10 and CelSC12 hydrogels and solutions were explored. Fibrous samples from CelSC10 and CelSC12 were also explored. Initial fluorescence experiments were performed at 5 °C. Then, spectra were acquired at 10 °C increments up to 75 °C for all samples except LacSC12, which was studied up to 85 °C. A front-face excitation-collection geometry was used for acquisition of hydrogel fluorescence spectra, since these materials are opaque at the lower temperatures. Preparation of hydrogel samples containing prodan for fluorescence spectroscopy consisted of first heating to the sol state, followed by pipetting the warm sol solution to fill a 1.7 mL triangular fluorescence cuvette (Wilmad Lab-Glass) which was then capped to prevent evaporation. Then, the cuvette was quenched at either room temperature or in an ice/water bath to form hydrogels or fibrous aggregates. Samples were then allowed to equilibrate for 30 min prior to measurement. Identical preparation was used for the 1 wt% LacSC8 and 1 wt% CelSC10 samples, both of which were visually clear and lacked any indication of turbidity, but fluorescence spectra were acquired on these sol solutions in a standard orthogonal excitation-collection fluorescence geometry in a 10 mm rectangular cuvette (Starna).

Fluorescence spectra were fit to a minimum number of 100% Gaussian bands needed to ensure a good fit. Peak

emission wavelengths and full-width-at-half-maximum (FWHM) values were unconstrained during fitting. Fits were deemed acceptable for χ^2 values >0.995.

X-Ray crystallography. Powder X-ray diffraction was performed on a Philips PANAlytical X'Pert PRO MPD X-ray diffraction system under Cu Kα X-ray radiation. The measurements were performed at room temperature using the Bragg–Brentano geometry.

Single crystal X-ray diffraction data for CelSC10 and CelSC12 were collected at 150 K on a D8 goniostat equipped with a Bruker PHOTON-II detector at Beamline 12.2.1 at the Advanced Light Source (Lawrence Berkeley National Laboratory) using synchrotron radiation tuned to λ = 0.7288 Å. For data collection, 1-s frames were measured in shutterless mode. APEX3 v2016.9.0 and SAINT v8.38A data collection and processing programs, respectively, were used. The Bruker Analytical X-ray Instruments, Inc. (Madison, WI) SADABS v2016.2 semi-empirical absorption and beam correction program (G.M. Sheldrick, University of Göttingen, Germany) was used. Using Olex2,[65] the structure was solved with the ShelXT structure solution program[66] using intrinsic phasing and refined with the ShelXL refinement package[67] using least squares minimization.

Results and discussion

Visual assessment of hydrogel formation

A wide range of thioglycolipid solutions were evaluated to establish concentration conditions (wt%) under which hydrogelation occurs and to assess the formation of other phases. Photographs of these hydrogels are shown in Fig. 1. Brief schematics describing hydrogel formation are shown in Fig. S19 (ESI†). Visual assessments of these aqueous solutions for different concentration conditions at room temperature are summarized in Table 1. In this table, C indicates clear solution devoid of any perceptible turbidity, O indicates turbid or cloudy solution, G indicates gel, G + C indicates a gel that has undergone syneresis over time, resulting after equilibration in a clear fluid layer on top of a gel, and F indicates the presence of fibers.

For LacSC8 and LacSC12 solutions at concentrations <0.5 wt%, the solutions are either clear (C) or turbid suggesting the presence of large aggregates (O). These solutions form partial hydrogels surrounded by clear solution between 0.5 but <1 wt% and are completely gelled at concentrations of 1 wt% and greater. Solutions of LacSC10 at <2 wt% form partial hydrogels surrounded by clear liquid but are completely gelled at or above 2 wt%.

CelSC8 solutions remain clear at all concentrations studied. When allowed to form at room temperature, CelSC10 and CelSC12 solutions form fibrous structures that settle out of solution after long periods of time or if they are subjected to even modest vibrational shock due to syneresis. However, CelSC10 and CelSC12 solutions can form hydrogels when rapidly quenched and maintained at temperatures <20 °C, although after warming to room temperature, these slowly transform into fibrous structures that settle out over time, suggesting that they are metastable in the gel state.

Substantial research on metastable LMWGs has been reported, and a universal energy level description of this behavior has emerged:[3,68–70] upon cooling from the solution state, aqueous samples containing amphiphilic gelators can be kinetically trapped in a metastable gel state, which prevents the molecules from forming crystals. In systems for which the activation barrier around the gel state is low, the system can transform into the crystalline state, as has been observed in many examples reported in literature.[3,51,68–73] Indeed, the balance of hydrophilic and hydrophobic intra- and intermolecular interactions is suggested to play the major role in dictating metastability,[3] although clear molecular design guidelines are still somewhat elusive.

In the work reported here, the gels from CelSC10 and CelSC12 demonstrate this gel-to-crystalline transition behavior indicative of a relatively low activation barrier out of the gel state. Indeed, X-ray diffractometry confirms the crystalline nature of these fibers (*vide infra*). However, when the barrier is sufficiently high, as is apparently true of the LacSC*x* gels, systems can be trapped in the gel state for longer periods, even indefinitely depending on the environmental conditions of the gel. Further evidence for metastability in the CelSC10 and CelSC12 gels is that when they are maintained at 5 °C after their formation at this temperature, the hydrogels are stable for over 6 months. The truly intriguing aspect of these observations is that this difference in energy landscape is conferred on these materials by a change in the configuration of only a single hydroxyl on the sugar distal to the alkyl chain at C4. In CelSC*x*, the hydroxyl at C4 in the sugar is equatorial (glucose) whereas in the LacSC*x* molecules, the hydroxyl at the C4 is axial (galactose). This distinction is discussed in greater depth below.

Overall, the minimum thioglycolipid concentration at which hydrogelation is observed can be as low as 0.05 wt% depending on thioglycolipid system. This compares favorably to the typical

Table 1 Visual assessment of aggregation and gelation behavior of thioglycolipids[a]

Thioglycolipid (wt%)	0.05	0.1	0.25	0.5	0.75	1	2	5	10
LacSC8	C	C	C	G + C	G + C	G	G	G	G
LacSC10	G + C	G + C	G + C	G + C	G + C	G + C	G	G	G
LacSC12	O	O	O	G + C	G + C	G	G	G	G
CelSC8	C	C	C	C	C	C	C	C	C
CelSC10	F	F	G or F	G or F	G or F	G or F	G or F	G or F	G or F
CelSC12	F	F	G or F	G or F	G or F	G or F	G or F	G or F	G or F

[a] C = clear solution, G + C = gel with clear liquid layer above, G = gel, O = cloudy solution, F = fibrous aggregate.

concentration for hydrogelation of similar low molecular weight systems of at least 1 wt% commonly reported in the literature, although 0.25–2 wt% is the concentration range wherein these thioglycolipid solutions fully hydrogel. The existence of metastable hydrogels and the ability to tune the transformation of hydrogels into crystals may allow their potential use as smart materials for different applications. Although LacSC*x* and CelSC*x* share almost identical chemical structure, the hydrogels from them exhibit very different properties. Therefore, the results and discussion of their properties below are separated for clarity. The properties of LacSC*x* (x = 8, 10, 12) hydrogels are detailed first followed by a discussion of the CelSC*x* (x = 10, 12) hydrogels and crystalline materials.

Thiolactoside hydrogels

Rheological properties. Rheology was employed to confirm the formation of hydrogels as well as to characterize the viscoelastic properties of these hydrogels. The two parameters of interest in these studies are storage modulus (G') and loss modulus (G''). Materials for which $G' > G''$ are considered viscoelastic solids, the common behavior for hydrogels; in contrast, systems for which $G'' > G'$ are considered viscoelastic liquids. The magnitude of G' as well as the viscoelastic and mechanical properties of the hydrogels are important parameters, as they dictate the utility of hydrogels in different applications. For instance, hydrogels used as carriers that release cargo such as fertilizer should have sufficient mechanical strength to withstand normal handling and storage without fracturing;[63] additionally, shear-thinning and thixotropic hydrogels with proper flow properties are better candidates for injectable therapeutic delivery vehicles.

Frequency sweep and strain sweep experiments (Fig. 2) were first conducted to explore the mechanical properties of the LacSC*x* hydrogels. Frequency sweep experiments were performed from 0.1 to 100 rad s^{-1} at a constant 0.01% shear strain, and strain sweep experiments were conducted from 0.1 to 1000% shear strain at a constant 10 rad s^{-1} angular frequency. LacSC8 and LacSC12 samples were at 1 wt% concentration, but LacSC10 was studied at 2 wt% given that it required higher concentration for full stable gelation. As shown in Fig. 2a, at 25 °C, dynamic frequency sweeps indicate that the LacSC8, LacSC10, and LacSC12 hydrogels exhibit solid-like behavior (*i.e.* $G' > G''$) that is invariant with frequency over the entire range of frequencies tested. Further, LacSC10 and LacSC12 hydrogels show large values of storage modulus (G') of $\sim 10^5$ Pa at 25 °C. Additional frequency sweep experiments at 4 and 10 °C were conducted and the results are shown in Fig. S20 (ESI†). These studies reveal that all LacSC*x* hydrogels demonstrate solid-like properties that are independent of frequency at all temperatures tested. Moreover, a trend of increasing G' values as temperature decreases is observed for LacSC8 and LacSC10 due to strengthening of the noncovalent interactions at lower temperatures. The G' values are also generally dependent on alkyl chain length with the G' for LacSC8 less than that for LacSC10 and LacSC12, which are close in value; these observations are not surprising, as longer alkyl chains are expected to result in stronger intermolecular interaction in the hydrophobic portion of these gels.

Fig. 2b shows the strain sweep results for LacSC8, LacSC10, and LacSC12 at 25 °C. These strain sweeps suggest that LacSC*x* hydrogels are stable viscoelastic solids (G' and G'' remain constant) when being deformed by <2% strain. This region of strain is known as the linear viscoelastic region, and it indicates the range wherein oscillatory strain can be applied without altering the structure of the material. As the strain becomes >2%, LacSC10 and LacSC12 hydrogels become unstable and the hydrogels move into the plastic deformation regime. Identification of this regime is useful for determining the shear strain limits for thixotropy experiments as described below.

In total, the LacSC*x* hydrogels demonstrate similar behavior, and the linearity limit and crossover points are generally independent of lipid alkyl tail length. Moreover, the mechanical properties of these hydrogels are qualitatively similar to those of most LMWGs reported in literature. However, the LacSC*x* hydrogels are distinct relative to other LMWGs by the relatively large magnitudes of their G' values. This distinction allows these gels to hold their shapes in liquids once molded. The G' values observed for the LacSC*x* gels at different temperature are given in Table S1 (ESI†).

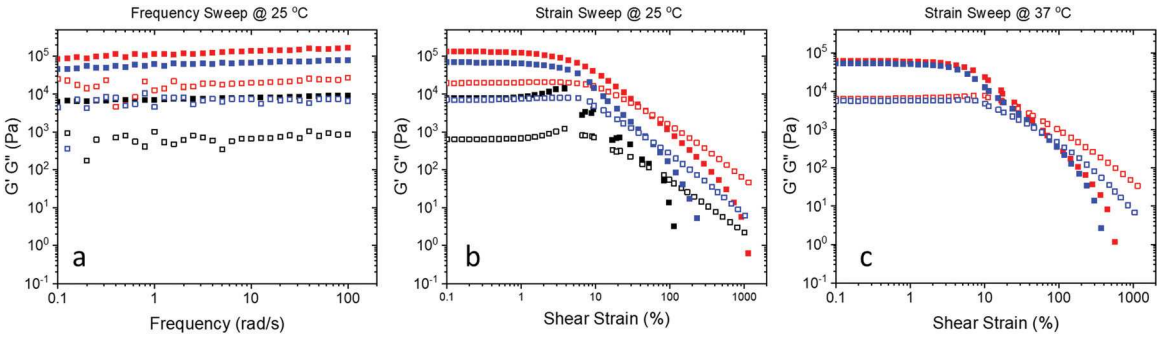

Fig. 2 Rheology results for 1 wt% LacSC8 and LacSC12 hydrogels and 2 wt% LacSC10 hydrogels. (a) Frequency sweep results and (b) strain sweep results at 25 °C, and (c) strain sweep results for LacSC10 and LacSC12 at 37 °C. Solid symbols (■, ■, ■) indicate G' values, open symbols (□, □, □) represent G'' values for LacSC8 (■, □), LacSC10 (■, □), and LacSC12 (■, □).

The LacSC*x* hydrogels described here exhibit G' values up to 10^5–10^6 Pa. In contrast to these values, typical G' values reported for peptide-based supramolecular hydrogels are in the range of 10^2–10^3 Pa,[74] with G' values reported for several sugar-based LMW hydrogels in the range of 10^0–10^5 Pa.[13,15,30,44,75] Monosaccharide-based hydrogelators with G' ranging from 10^2–10^4 Pa have been reported by Wang,[76,77] while Latxague *et al.* reported a biopolar glycolipid based hydrogel that exhibits G' values as high as 10^4 Pa.[13,15] Sekhar and coworkers prepared a series of glycolipid-based LMWGs based on *N*-methyl-D-glucamine with branched asymmetrical and symmetrical octadecyl chain hydrocarbon tails containing 0, 1, 2 or 3 sites of unsaturation that exhibited G' values ranging from 2 to 10^3 Pa.[44,78] Ben and coworkers reported hydrogels from *N*-octyl-D-gluonamide that have G' values in the range of 10^4–10^5.[30] Yamanaka and coworkers recently reported several lactose and maltose-based hydrogelators with G' values of 10^3–10^4 Pa.[47,48] Thus, the values of G' for the LacSC*x* hydrogels rank among the highest observed for LMWGs, suggesting that, despite their simple chemical structures compared with other sugar-based hydrogelators, the 3D networks of the LacSC*x* hydrogels are unexpectedly strong.

Fig. 2c shows the strain sweep results for LacSC10 and LacSC12 at 37 °C. The corresponding frequency sweep information is shown in Fig. S20 (ESI†). Interestingly, the LacSC10 and LacSC12 properties do not change much from those at 25 °C, although a small drop in G' value for LacSC10 is observed. Among all hydrogels tested, only LacSC10 and LacSC12 retain their hydrogel properties at 37 °C or higher temperature for more than 24 h. Further mechanical strength and stability at 37 °C can be achieved for LacSC12 at a slightly higher concentration of 2 wt% (see Fig. S21, ESI†). This stability at physiological temperature makes these materials suitable for possible applications as biomaterials.

Thixotropic materials[79] are desirable when it comes to certain applications of hydrogels in the food industry, cosmetics, and biomedical science. In addition, thixotropic LMWGs have gained considerable attention for their potential use in drug delivery and other pharmaceutical applications. Therefore, to explore further the potential utility of the LacSC10 and LacSC12 materials at physiological temperature, thixotropy experiments were performed in which the shear strain is stepped between 0.01 and 100% to evaluate the self-healing properties of these gels at 37 °C. The results are shown in Fig. 3. At 0.01% strain, these gels exhibit G' values greater than their G'' values. Upon stepping the strain to 100%, both G' and G'' values decrease in magnitude, with the G' values decreasing more than the G'' values. As a result, the G'' value becomes greater than the G' value, indicating the transition to a viscoelastic liquid state at 100% strain. Noteworthy is that this change is observed essentially instantaneously (*i.e.* within the measurement period of 10 s) for LacSC10. However, for LacSC12, this decrease takes 10's of sec for G'' with G' values continuing to decrease after the strain step indicating that the process is more kinetically limited given the stronger intermolecular interactions of the longer chain length. Upon stepping the stain back down to 0.01%, both LacSC10 and LacSC12 almost immediately regain their initial G' and G'' properties, confirming that the gels self-heal at a rapid rate.

Although other thixotropic gels are reported in literature, their properties vary considerably in terms of molecular structure, rheology, and microstructure (fibrous, porous, discs), making comparison with these LacSC10 and LacSC12 gels difficult. However, a common observation regarding the microstructure of several sugar-based thixotropic gels[13,15] is that these gels are generally fibrous, possessing microstructures with specific junction zones that hold the gel structure together. These junctions are the weak points within these gels and break under increased shear but recover with time when shear is removed. Although the microstructures of the LacSC10 and LacSC12 gels studied here are not fibrous, the intermolecular interactions holding the gels together are clearly reversible, a property that may be used to avail in certain applications requiring gel flow.

Microstructure of xerogels by electron microscopy. One of the most unpredictable and perplexing aspects of LMW hydrogel formation is the self-assembly process, which is usually estimated from hydrogel microstructure, because it provides

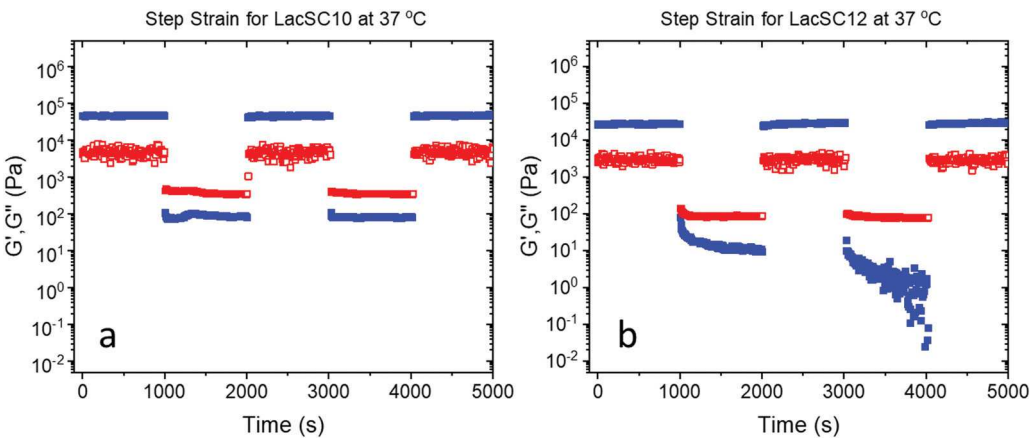

Fig. 3 Step-strain experiment for (a) 2 wt% LacSC10 and (b) 1 wt% LacSC12 hydrogel at 37 °C. (■) indicates storage modulus (G'); (□) indicates loss modulus (G'').

insight into the intermolecular interactions that lead to formation of the hydrogel network. Freeze-fracture SEM and TEM are the most commonly used approaches for investigation of hydrogel microstructure. In this approach, a xerogel of the hydrogel is first made by flash freezing the gel in liquid N_2 followed by lyophilization to remove water or solvent.[80] The xerogel so formed can then be studied with standard SEM and TEM. Admittedly, the resulting xerogel structure might fail to completely represent hydrogel microstructure because of changes that occur during the flash freezing and lyophilization processes. However, this approach is generally accepted to reflect hydrogel microstructure and so was used here to reveal structural details in xerogels on a scale of 100's of nm to μm. Hydrogel samples from the LacSC*x* systems and the metastable hydrogels from CelSC10 and CelSC12 were investigated. Xerogels and fibrous structures resulting from precipitation of the metastable CelSC10 and CelSC12 systems were also analyzed which are discussed in later sections.

Fig. 4a–l show representative SEM images of xerogels at different magnifications from the LacSC*x* systems at the wt% indicated. These xerogels consist of a layered structure of rumpled sheets of thioglycolipid that are strongly suggestive of sheet stacks in which the thioglycolipids are packed in lamellar structures based on bilayers of thioglycolipid. Glycolipids are well-known to pack in lamellar and curved lamellar structures (*e.g.* cubic) with their liquid crystalline phases existing as the related smectic A_d phase.[34,50,52,53,81–84] Higher magnification of individual sheets (Fig. 4d and h) confirms this structure. Although the size of each sheet varies widely, it is clear that these sheets can span areas as large as 10's of μm by 10's of μm. On a μm scale, wrinkled and wavy layers are observed (see Fig. 4d and f–h) Interestingly, more folds are observed in these structures in going from LacSC8 to LacSC10 to LacSC12. This observation suggests that hydrophobic interactions may drive fold formation, and by extension, may ultimately be the forces that balance gel formation and eventual crystallization through the formation of cylindrical fibers.

In several images, small amounts of amorphous or crystalline LacSC*x* structures are also observed at apparently random sites throughout the matrix. These structures clearly do not contribute to the hydrogel network but may be thioglycolipids that have begun to crystallize out of the hydrogel. Whether this occurs within the hydrogel as it exists or during the flash-freezing and lyophilization processes of making the xerogels is unclear; however, the presence of these structures suggests that the hydrogel is a metastable state with crystallization possible, albeit with a high barrier based on the stability of these gels.

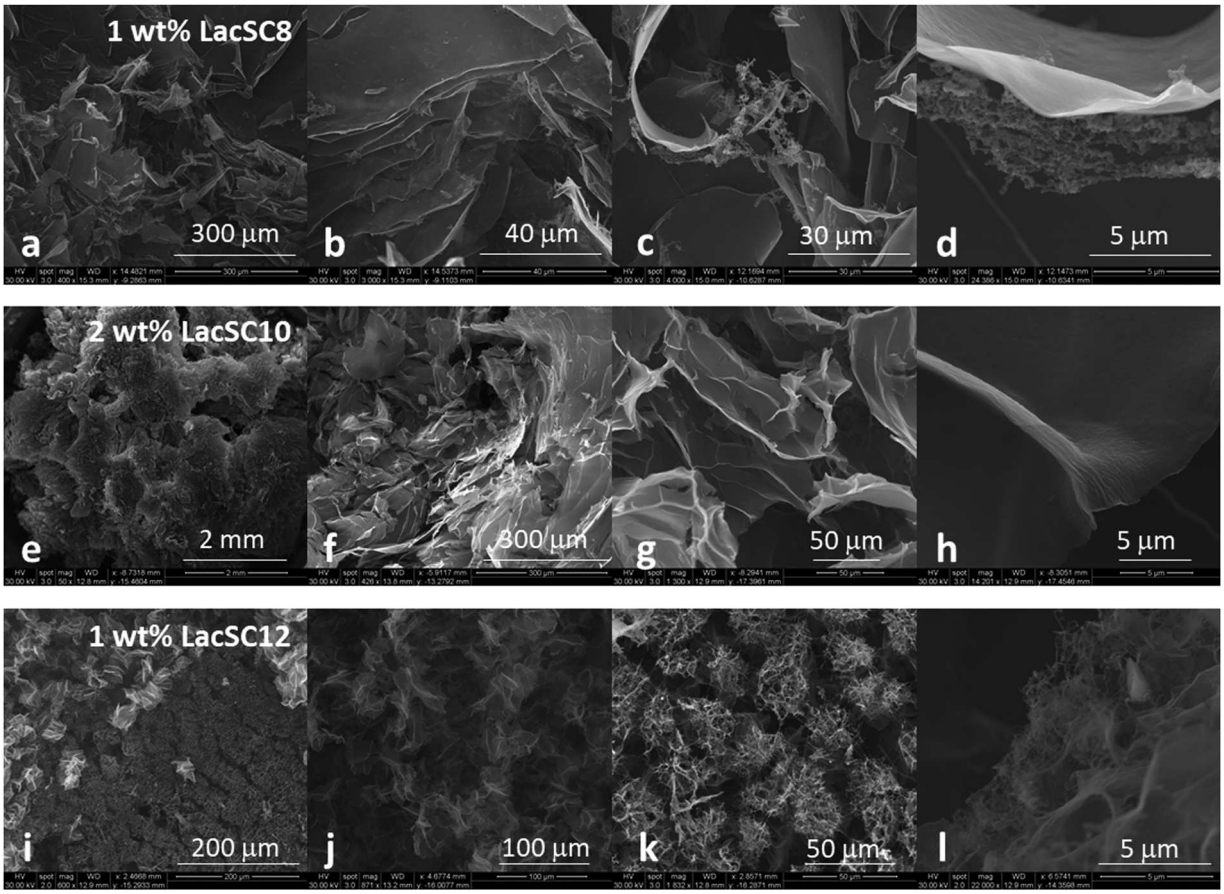

Fig. 4 Scanning electron micrographs of xerogels at different magnifications from flash freezing and lyophilizing hydrogels of (a–d) 1 wt% LacSC8, (e–h) 2 wt% LacSC10, and (i–l) 1 wt% LacSC12.

Although the layered structures of the xerogels are revealed by SEM, additional details on a size scale of 10's of nm would be useful to assess whether the structures observed in the SEMs are, in fact, a tertiary structure composed of smaller secondary and primary structures of the thiolactoside monomers. Hence, TEM was used on LacSC10 xerogels, as representative of the stable LacSC*x* hydrogels, supported on carbon grids to further investigate the nanostructure of these materials. We note that the samples thin enough to be suitable for TEM had to be prepared using a different protocol than used for the xerogels studied by SEM. TEM samples were prepared by depositing a thin film from hexane which was then allowed to evaporate prior to analysis. This process is substantially different from that used for the SEM images in which the aqueous hydrogels were flash frozen and lyophilized. The possibility thus exists that the resulting microstructures of the xerogels studied by TEM differ from those studied by SEM as the result of these differences in preparation.

Fig. 5a shows TEM images acquired in the annular dark field mode at relatively low magnification. In this image, layered structures that are observed in the SEM images are clearly apparent. At higher magnification, Fig. 5b and c show TEM images from the LacSC10 xerogel at nm spatial resolution, with the image in Fig. 5b acquired in the annular dark field mode but Fig. 5c acquired in the secondary electron mode at the same position as Fig. 5b. The difference between the two acquisition modes is that the annular dark field mode (Fig. 5b) shows structural information throughout the thin film whereas the secondary electron mode (Fig. 5c) shows structural features only from the surface of the film facing the electron beam. Fig. 5b and c both show the presence of pores randomly distributed in the xerogel structure. Fig. 5b documents that these pores exist throughout the film. However, Fig. 5c shows large regions of what appear to be closely packed lamellar structures on the surface of the thin film, suggesting that the pores may result from what can be described as a disordered bicontinuous cubic phase based on lamellar bilayers of the thioglycolipids. Overall, the TEM images do not show any obvious aggregation pattern of LacSC10 beyond layered sheets of intrinsically lamellar structures.

As a final caveat to the election microscopy results, it is again noted that xerogel structures might not represent hydrogel microstructures due to artifacts caused by drying. Nonetheless, these electron microscopy results differ substantially from the fibrous structures of xerogels observed for the alkyl thiocellobiose systems (*vide infra*) and more commonly reported. These results are thus intriguing, as the microstructures of most previously studied LMWGs are either entangled fibrils or entangled ribbons.

Gel-to-sol transition temperatures by DSC. After visual assessment of gelation properties as a function of concentration and temperature, differential scanning calorimetry (DSC) was used to determine the gel-to-sol phase transition temperatures more accurately as well as to look for other potential lyotropic phases. The results of these studies are summarized in Table 2.

The gel-to-sol phase transition temperatures measured with DSC can be used as an additional quantitative indicator of hydrogel stability; DSC further enables determination of the enthalpy change during this phase transition. In the temperature range from 5 to 85 °C, within which water remains liquid, an endothermic process is observed for each hydrogel, with the transition temperature increasing anywhere from 10–25 °C for each two-carbon increase in alkyl chain length. The transition temperatures measured with DSC match those observed visually in bulk mixtures. Unsurprisingly, hydrogels made from thioglycolipids with longer carbon chains have higher thermostability (*e.g.* higher phase transition temperature). LacSC8 and LacSC10 gels require almost identical enthalpies for the gel-to-sol transition whereas LacSC12 hydrogels require twice as much enthalpy. This suggests that as alkyl chain length increases, greater thermal stability is conferred on the hydrogels in a nonlinear fashion. Overall, the magnitude of the enthalpy changes observed is relatively small. This is rationalized by the fact that the hydrogel structure does not break into free monomers upon gel-to-sol transition, but instead, the macroscopic hydrogel structure transforms into nanoscale aggregate units in solution. Such structures retain a considerable fraction of the hydrophobic bonding strength of the lamellar structures, but exist as many isolated entities instead of a macroscopic network.

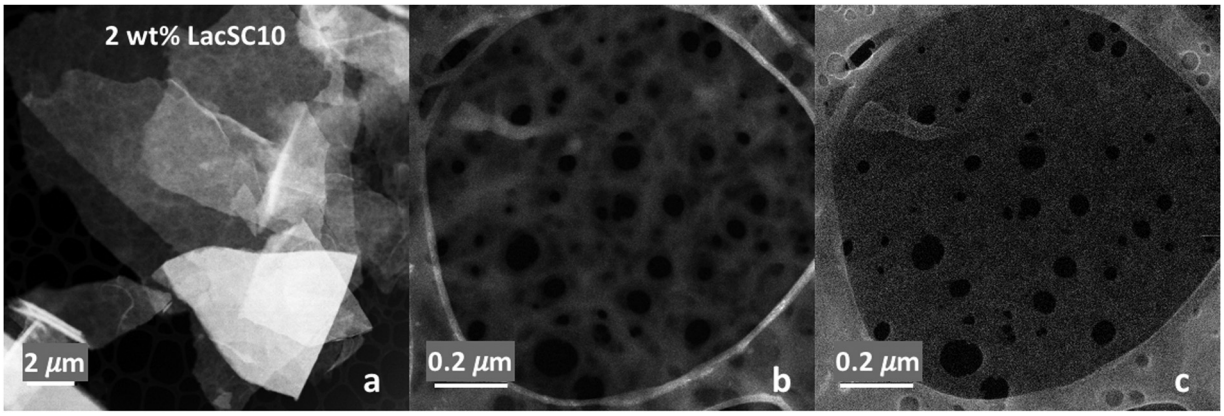

Fig. 5 Transmission electron micrographs from 2 wt% xerogels of LacSC10 at two different magnifications; (a) and (b) acquired in annular dark field mode and (c) acquired in secondary electron mode. Scales bars in each case represent (a) 2 μm, and (b and c) 0.2 μm.

Table 2 Differential scanning calorimetry results for LacSC*x* and CelSC*x* systems

Thioglycolipid	T_g (°C)[a]	Enthalpy (J g^{-1} hydrogel)	Enthalpy (kJ mol^{-1} thioglycolipid)
1 wt% LacSC8	38	0.196 ± 0.030	9.21 ± 1.41
2 wt% LacSC10	64	0.354 ± 0.022	8.83 ± 0.54
1 wt% LacSC12	79	0.392 ± 0.100	20.7 ± 5.3
1 wt% CelSC10	37	0.180 ± 0.013	8.99 ± 0.64
1 wt% CelSC12	47	0.424 ± 0.063	22.3 ± 3.3

[a] T_g = Temperature of gel-to-sol transition.

Prodan fluorescence for lyotropic phase identification. Further insight into the structure and microenvironment of these thioglycoside systems at different temperatures and concentrations is provided by fluorescence spectroscopy using the polarity-sensitive fluorophore, prodan. Work by Karukstis *et al.* has demonstrated that the peak emission wavelength for prodan reports on the polarity of its microenvironment, thereby providing information about the nature of the amphiphile aggregation.[85] The emission maximum shifts to shorter wavelengths with increasing order due to a decrease in polarity of the environment of the sequestered prodan. The emission maximum for prodan free in aqueous solution is 525 nm; this systematically decreases with increasing order through micellar (M), hexagonal (H), lamellar (L), cubic (C), gel (Gel) and crystalline (Cry) phases. For the various lyotropic phases of octyl glucoside, the peak emission wavelengths and corresponding microstructures were reported as follows:[85]

Structure	Cry <	Gel <	C ≪	L <	H <	M <	H_2O
λ_{prodan} (nm)	380	400	410	473	485	490	525

The polarity-sensitive property of prodan was used here to assess changes in microenvironment within these aqueous thioglycolipid mixtures with concentration and temperature. Spectra at representative concentrations for the LacSC*x* series as a function of temperature are shown in Fig. 6. Spectra for all LacSC*x* concentrations studied are shown in Fig. S21–S23 (ESI†).

Fig. 6a–c reveal several similarities across the three LacSC*x* (*x* = 8, 10, 10) systems. First, at temperatures lower than the gel-to-sol transition temperature (*i.e.* 38 °C for LacSC8, 64 °C for LacSC10, and 79 °C for LacSC12), a major emission band was observed with a peak of 478–491 nm. In interpreting these spectra, it is important to recall that they reflect the spectral response from the entire hydrogel, including the water phase and the more solid-like phase. Since the water phase is the major component of these hydrogels, it is reasonable to attribute the major band at 478–491 nm to prodan in micellar aggregates in the aqueous phase of the hydrogel as we have observed for related thioglycolipids.[49] An additional peak in the wavelength range of 421–428 nm is observed for higher concentration samples of LacSC8 (see Fig. S22, ESI†) and all concentrations of LacSC10 and LacSC12 in the hydrogel state. This additional band is in between the peak wavelengths identified by Karukstis for the cubic and lamellar phases[85] and is attributed here to prodan that is fully embedded within the thioglycolipid microstructure of the hydrogels in an environment that resembles something between an ordered cubic phase and a lamellar phase based on its peak wavelength. This assignment is wholly consistent with the conclusion of a disordered bicontinuous cubic phase based on thioglycolipid lamellar bilayers from the electron microscopy studies. Further evidence for these assignments comes from heating these LacSC*x* hydrogels above their gel-to-sol transition temperatures wherein the thiolactosides are in the sol state, whereupon the prodan fluorescence exhibits a dominant emission peak at 487–500 nm assigned to prodan in smaller LacSC*x* micellar aggregates.

The prodan peak emission wavelengths were extracted from these fluorescence spectra by band decomposition. All prodan fluorescence spectra from the LacSC*x* systems (Fig. S22–S24, ESI†) can be fit with only two bands, indicating only two phases, in the temperature range from 5 to 85 °C. The spectral fits for all LacSC*x* systems are shown in Fig. S25 (ESI†), the peak emission wavelengths are given in Table 3, and the FWHM of the fit peaks in Table S2 (ESI†). Based on the maximum emission wavelengths, these are assigned to disordered bicontinuous cubic/lamellar and micellar phases. Similarly, in analyses of spectral data from the LacSC8 and LacSC10 systems up to 10 wt% (Fig. S22 and S23, ESI†), only two major lyotropic phases are observed, disordered bicontinuous cubic/lamellar phase, which is only observed at temperatures below the gel-to-sol transition, and the micellar phase, which is observed both for temperatures below and above the transition. The behavior is generally similar for the LacSC12 system, except for the observation of a small band at 520 nm for temperatures above the gel-to-sol transition. This additional band is assigned to prodan free in solution and indicates that melting of the hydrogel creates a mixed solution of phase-separated LacSC12 sols that exclude some fraction of the prodan. Despite this anomaly, the micellar states for all LacSC*x* samples are generally stable up to 85 °C. In total, these prodan fluorescence spectra support the conclusions based on electron microscopy of xerogels of disordered bicontinuous cubic structures based on lamellar bilayers in hydrogels of LacSC*x*.

Estimated phase diagrams for LacSC*x* systems. Combining the results gleaned from the collective set of studies described above, phase diagrams were estimated for each of the LacSC*x* systems. These are shown in Fig. 7. The phase boundary lines in each case serve only as guides to the eye based on experimentally determined data points shown by the colored symbols.

Typical phase diagrams of amphiphilic molecules or surfactants include mainly three regions: solid, monomers and micelles. The solid phase usually lies in the low temperature/high concentration range and represents the concentration and temperature range wherein the surfactant is not soluble in the solvent and either phase separates or precipitates. The monomer region usually lies in the low concentration range across all temperatures. In this range of concentration and temperature, the surfactant molecules are

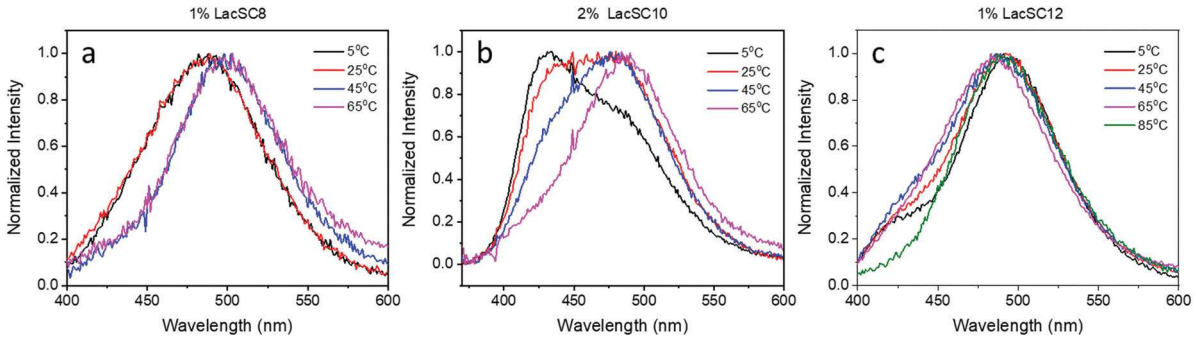

Fig. 6 Steady-state fluorescence spectra from prodan-doped LacSC*x* hydrogels at representative temperatures: (a) 1 wt% LacSC8, (b) 2 wt% LacSC10, and (c) 1 wt% LacSC12.

Table 3 Emission maxima indicative of different lyotropic phases for LacSC*x* from spectral fitting of prodan fluorescence spectra at room temperature and at a temperature above the gel-to-sol transition

	T = 25 °C		$T > T_g$ [a]	
LacSC*x*	λ_1 (nm)	λ_2 (nm)	λ_1 (nm)	λ_2 (nm)
LacSC8	—	484	500	—
LacSC10	428	478	493	—
LacSC12	421	491	487	520

[a] T_g is gel-to-sol transition temperature. Measurement temperatures for LacSC8 and LacSC10 : 75 °C, for LacSC12 85 °C.

soluble in the solvent but not at concentrations high enough to drive aggregation and micelle formation. For concentrations above the critical micelle concentration (CMC), surfactants begin to aggregate into different lyotropic phases in solution depending on temperature. The phase diagrams estimated here can be understood with similar logic. The hydrogel network is viewed as a solid phase in which the thioglycolipids extensively aggregate. For LacSC*x* (x = 8, 10, 12), this is a viscoelastic solid comprised of macroscopic sheets of a disordered bicontinuous cubic phase of lamellar bilayers in which the molecules are not in the crystalline state but are highly organized. This hydrogel region lies in the low temperature range but doesn't exist at low concentrations. As temperature increases, the hydrogels "melt" into the micellar or sol state. This gel-to-sol transition is where the temperature exceeds the solubility line with formation of either monomers, micelles, or phase separated regions. Because the concentrations studied here greatly exceed the CMC values, we observe only lyotropic phases in the LacSC*x* systems.

Thiocellobioside hydrogels

As noted above, thiocellobiosides form metastable hydrogels as well as fibrous samples. Table 4 summarizes the visual observations of the CelSC*x* (x = 10, 12) samples after 24 h equilibration at different temperatures. When a mild vibrational perturbation is applied to the CelSC*x* hydrogels, they slowly transform into fibrous crystals. However, without perturbation, the CelSC12 fibrous hydrogel remains somewhat stable even at 35 °C.

Generally, when the CelSC*x* materials are in the metastable hydrogel state, they exhibit characteristics and properties similar to those of the LacSC*x* (x = 8, 10, 12) hydrogels. However, due to their instability at temperatures of 25 °C and greater, rheology was performed only at 4 °C at which the CelSC*x* hydrogels are stable. These results are shown in Fig. 8. The lower stability of the CelSC10 and CelSC12 hydrogels is confirmed by the lower G' values ($\sim 10^4$ Pa) observed compared to those of the LacSC10 and LacSC12 hydrogels ($\sim 10^5$ Pa). This behavior is interesting given the equivalent alkyl chain lengths with only subtle differences in chemical structure.

Fig. 9a–d show SEM images of xerogels formed from the metastable thiocellobioside hydrogels. CelSC*x* hydrogels

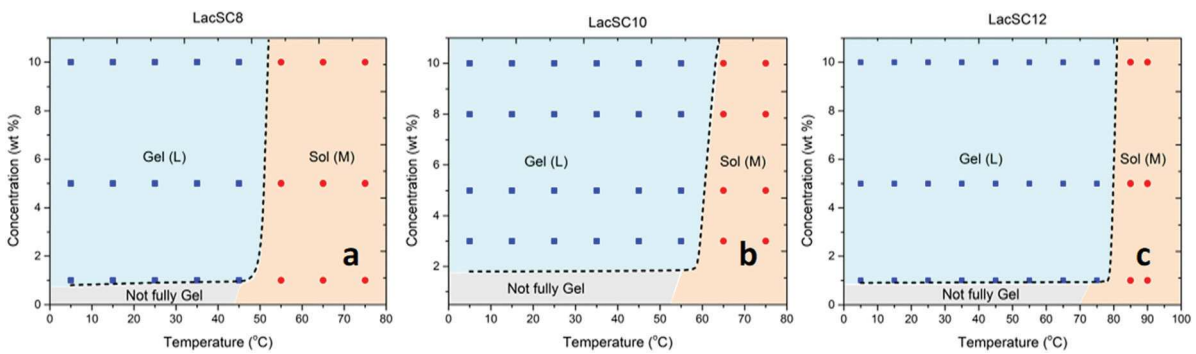

Fig. 7 Phase diagrams estimated for (a) LacSC8, (b) LacSC10, and (c) LacSC12. Phase boundary lines are guides to the eyes based on experimentally determined data points shown as colored symbols. ■ = gel; ● = sol.

Table 4 Visual observation of CelSC10 and CelSC12 samples at different temperatures after equilibration for 24 h

	CelSC10		CelSC12	
T (°C)	Without perturbation[a]	With perturbation	Without perturbation	With perturbation
5	G[b]	F	G	F
25	F	F	G	F
35	F	F	G	F
45	F	F	F	F
65	S	S	S	S

[a] The perturbation applied is a mild vibrational shock. [b] G = gel; F = fibrous aggregate, S = sol.

possess the folded sheet microstructure similar to that of the LacSC*x* hydrogels (Fig. 4b and g) with small inclusions of amorphous or crystalline aggregates. At higher magnification, Fig. 9b suggests a similar porous nature of the sheet as observed in the TEM images from the LacSC10 hydrogels (Fig. 5c). SEM images taken on the metastable CelSC*x* hydrogel samples suggest similar aggregation behavior in the CelSC*x* and LacSC*x* systems; this is generally unsurprising in light of their structural similarities.

DSC analysis of CelSC10 and CelSC12 hydrogels (Table 2) indicates a lower tolerance to melting than the LacSC*x* hydrogels of similar alkyl chain length, with phase transition temperatures of 37 and 47 °C for CelSC10 and CelSC12, respectively, compared with temperatures of 64 and 79 °C for the corresponding LacSC*x* systems. Despite these lower phase transitions temperatures, however, no significant difference in enthalpy is noted for the CelSC*x* gel-to-sol transitions than for the LacSC*x* gel-to-sol transitions.

Prodan fluorescence was also employed to understand the aggregation of CelSC*x*. These spectra are shown in Fig. S26 (ESI†) with the spectral fits shown in Fig. S27 (ESI†). As noted above, CelSC10 hydrogels turn into fibrous aggregates readily at and above room temperature, although fluorescence spectroscopy of the metastable CelSC10 hydrogels could be performed at temperatures <15 °C. At the warmest temperature at which the CelSC10 hydrogels could be maintained ($\sim$15 °C), prodan fluorescence in the CelSC10 hydrogel exhibits a major emission band at 486 nm, similar to that observed for the LacSC*x* hydrogels. As above, this band is assigned to prodan in micellar

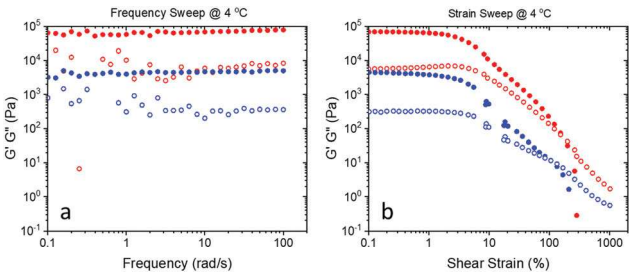

Fig. 8 Frequency sweep and strain sweep results at 4 °C for 1 wt% CelSC10 and 1 wt% CelSC12 hydrogels. Solid symbols (●, ●) represent G' values and open symbols (○, ○) represent G'' values for CelSC10 (●, ○) and CelSC12; (●, ○).

structures in the aqueous phase of the hydrogel. These metastable hydrogels have a weak band at 436 nm similar to that observed for the LacsSCx gels assigned to a disordered bicontinuous cubic phase based on lamellar bilayers. In contrast, prodan fluorescence spectroscopy from the CelSC10 fibrous state at temperatures below the gel-to-sol transition are dominated by the emission band at 436 nm with only a small shoulder at 486 nm (Fig. S26, ESI†). The peak at 436 nm is assigned to prodan located within the fibers.

The hydrogel state for CelSC12 behaves somewhat differently. CelSC12 hydrogels are relatively stable, cloudier, and remain as metastable hydrogels to 35 °C for at least 24 h if not subjected to any vibrational perturbation (Table 4). Prodan fluorescence spectroscopy was performed on these hydrogels (Fig. S26–S29, ESI†), and at temperatures below the gel-to-sol transition, the spectra are dominated by a peak at 492 nm, similar to what is observed for the LacSC*x* hydrogels (Tables S2 and S3, ESI†). This similarity supports the assertion that the CelSC12 hydrogels aggregate similarly to the LacSC12 hydrogels.

At temperatures above the gel-to-sol transition, both the CelSC10 and CelSC12 systems behave identically to the LacSC*x* materials in that a major peak is observed at 489–495 nm that is assigned to the micellar or sol phase with a smaller peak at 520–525 nm that is assigned to prodan free in solution. In brief, as long as the CelSC*x* materials remain in the metastable hydrogel state, they exhibit properties similar to the LacSC*x* hydrogels, possessing identical microstructure and aggregation patterns but with weaker mechanical properties and lower tolerance to heat.

Further insight into the microstructure of the fibrous CelSC*x* samples is provided by SEM. Fig. 9e–k show SEM images of the fibrous samples from CelSC10 and CelSC12. These materials primarily consist of fibrils that resemble crystals with a small amount of layered structures observed (Fig. 9f and j). The presence of small amounts of the layered structure is consistent with the prodan fluorescence results that indicate residual hydrogel that has yet to crystallize into fibers. This may explain why the fibers can retain their shape after transitioning out of the hydrogel structure even when placed upside down. Comparison of the SEMS of the hydrogels (Fig. 9a–d) and fibrous systems (Fig. 9e–k) reveals that the microstructure can be very diverse, consistent with the idea that the gelation process is metastable, representing a competition between aggregation into a lamellar hydrogel network and crystallization into a fibrous morphology.

To ascertain whether the fibers that form from the gel state are indeed crystalline, both powder X-ray diffraction and synchrotron-based single crystal X-ray crystallography were performed on fibers crystallized and harvested directly from gel samples. These fibers were not subjected to any drying process prior to their XRD analysis. The powder X-ray diffraction results are shown in Fig. S30 (ESI†) for 1 wt% CelSC10 and CelSC12. The multitude of sharp peaks in the 2θ data are clearly indicative of crystalline materials. Single crystal X-ray crystallography on these very fine fibers was performed using

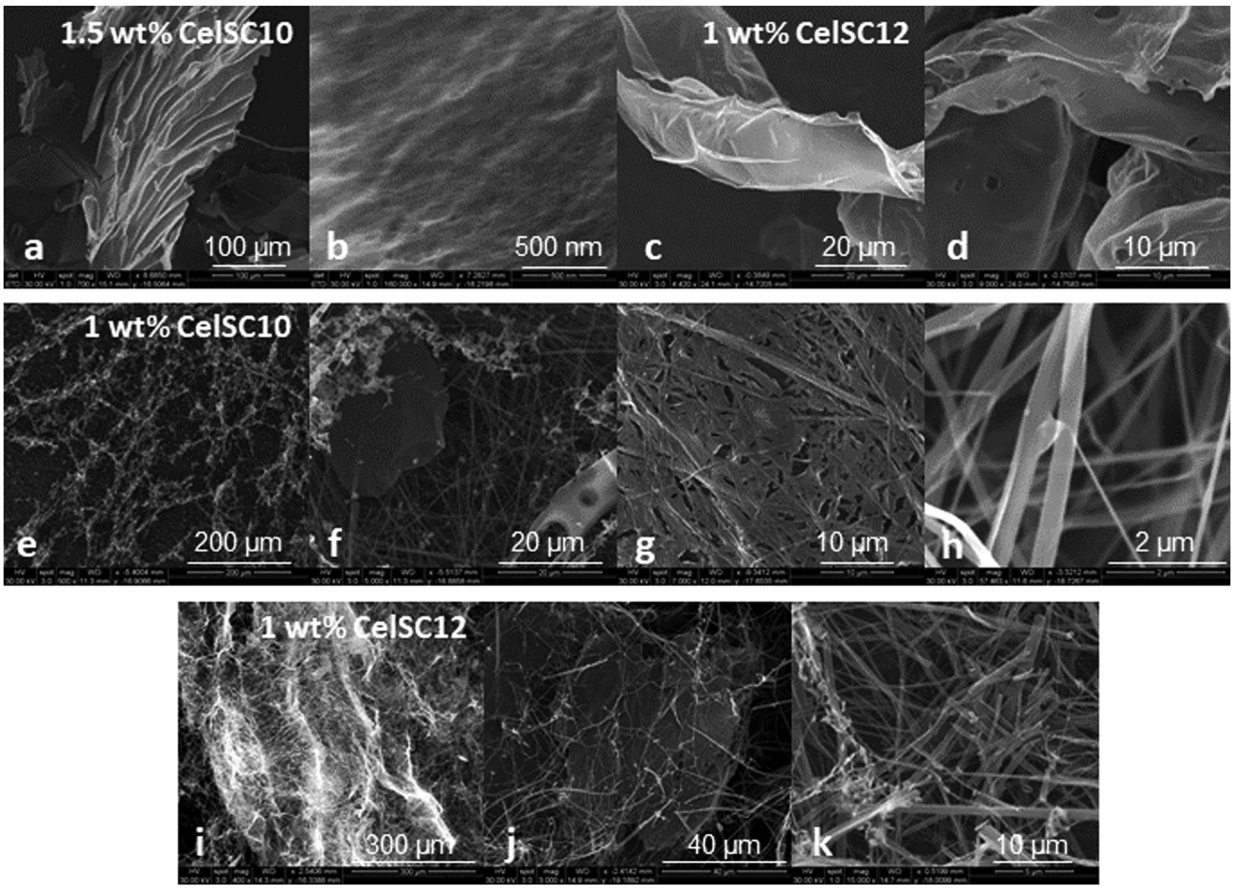

Fig. 9 Scanning electron micrographs at different magnification of xerogels from flash freezing and lyophilizing hydrogels of (a and b) 1.5 wt% CelSC10, (c and d) 1 wt% CelSC12, (e and h) 1 wt% CelSC10 fibers, and (i–k) 1 wt% CelSC12 fibers.

synchrotron radiation at the Advanced Light Source; these data are summarized in the ESI† with crystal structures shown in Fig. S31 and S32. These structures show that CelSC*x* crystals are layered with the sugar headgroups in rows of head-to-head orientation along the outside of interdigitated alkyl tails, similar to what has been observed previously for crystalline and liquid crystalline alkyl glycolipid structures.[34,50,86–90] Of note is that the CelSC*x* materials crystallize out as the dihydrates from these dilute solutions wherein the water molecules play a significant role in stabilization of the structure through hydrogen bonding. Previous work has shown that octyl-α-D-glucopyranoside can crystallize as the mono- or hemihydrate,[89] but we have found no evidence of dihydrates of alkyl glycolipid crystalline materials reported in the literature. Although this molecular packing pattern in the single crystals does not necessarily represent the aggregation pattern of molecules in the hydrogel structures, it does provide some possible insight into the different properties of the two types of hydrogel systems observed here. More specifically, the crystal structures of the CelSC*x* materials allow consideration of what interactions might provide their lower barrier to crystallization. Indeed, previous work on the lyotropic phases of the *O*-linked systems of β-GlcC8 and β-GalC8 has shown differences in crystalline lamellar phase structure in going from Glc to Gal; a smaller layer spacing by 4 Å was observed for crystalline β-GalC8 compared with crystalline β-GlcC8 and was attributed to greater interdigitation of the chains and consequently stronger interchain hydrophobic interactions.[34] In the disaccharide-based CelSC*x* and LacSC*x* systems studied here, it seems unlikely that a significant difference in interchain spacing occurs. However, careful analysis of the CelSC*x* crystal structures reveals the presence of a critical bridging hydrogen bonding configuration between the C4 equatorial hydroxyl on the distal Glc of the Cel headgroup with an integral water of the crystal structure. In the corresponding LacSC*x* systems, the axial configuration of the C4 hydroxyl would disallow this hydrogen bonding interaction. We speculate that this difference in configuration of the C4 hydroxyl in Cel results in a critical stabilizing hydrogen bond that decreases the barrier out of the metastable hydrogel state for the CelSC*x* systems but not the LacSC*x* systems. Thus, the CelSC*x* systems more rapidly convert to their corresponding crystalline phases while the LacSC*x* systems remain trapped in the gel state.

Using the data in hand for the CelSC*x* (x = 8, 10, 12) materials, phase diagrams for each system were estimated and are shown in Fig. 10. Again, it is important to note that the phase boundary lines are only used as guides to the eye based on experimentally determined data points shown by the colored symbols. These phase diagrams exhibit substantial

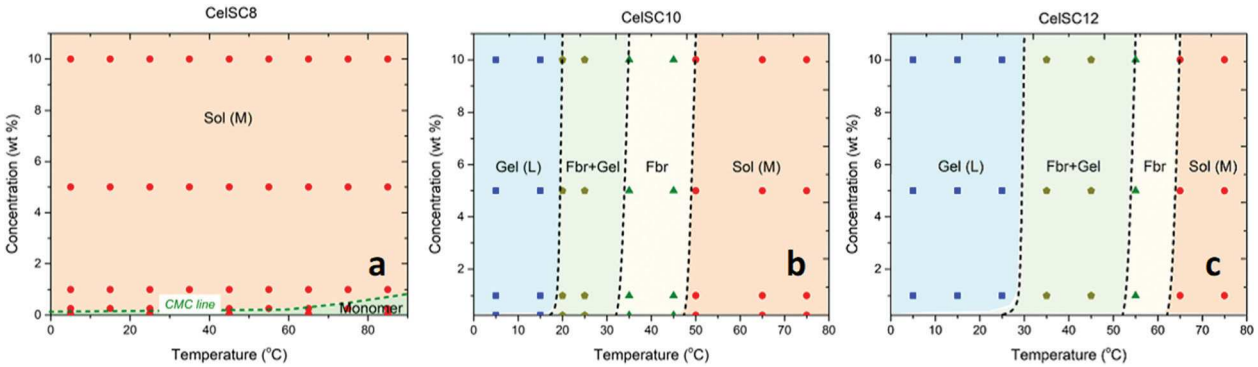

Fig. 10 Phase diagrams estimated for (a) CelSC8, (b) CelSC10, and (c) CelSC12. Phase boundary lines are guides to the eyes based on experimentally determined data points shown as colored symbols. ■ = gel; ⬟ = gel + fibers; ▲ = fibers; ● = sol.

similarity to those for the LacSC*x* systems. At temperatures above the gel-to-sol transition, the micellar state dominates. For CelSC8, this is the only phase observed at all temperatures studied. In contrast to the LacSC*x* systems, however, two states exist for the CelSC10 and CelSC12 systems below the solubility line; these are hydrogel and fibrous crystalline state, with both representing a different form of aggregation out of aqueous solution. At low temperatures, the CelSC10 and CelSC12 hydrogels can be stable for weeks if not months. However, for temperatures above ~15 °C for CelSC10 and ~25 °C for CelSC12 up to the gel-to-sol transition temperature, these hydrogels slowly crystallize into fibers in a few days, indicating that the hydrogels are metastable.

Conclusions

LMWGs have attracted considerable interest in the materials community, and many studies have focused on utilizing sugar containing LMWGs for various applications. We have synthesized two classes of disaccharide-based thioglycolipids hydrogels and characterized their physical properties. LacSC8, LacSC10, and LacSC12 form stable hydrogels at room temperature; the LacSC10 and LacSC12 hydrogels are stable to 64 and 79 °C, respectively, making them potentially of interest for biomaterials applications. CelSC10 and CelSC12 form metastable hydrogels with gel-to-sol transition temperatures of 31 and 42 °C, respectively, but they are only metastable and slowly transform into crystalline fibers at room temperature. However, CelSC10 and CelSC12 hydrogels do remain stable for more than 6 months when kept at 5 °C. Rheology demonstrates that the LacSC*x* hydrogels exhibit excellent mechanical properties with storage moduli up to almost 10^6 Pa. In addition, thixotropic characteristics are exhibited by the LacSC10 and LacSC12 hydrogels. SEM and TEM images of xerogels of these hydrogels reveal a microstructure comprised of a layered 3D network that appears to be made of a disordered bicontinuous cubic phase of lamellar bilayers. Fluorescence spectroscopy of the microenvironment-sensitive dye prodan is also consistent with this microstructure. Not only are these hydrogelators synthesized in a straightforward, cost-effective, high yield process, these materials represent a new class of sugar based LMWGs that possess high G' with intriguing microstructures that suggest their potential use in a myriad of applications. The linear β (1 → 4) linkage in the Lac and Cel headgroups confer unique structural efficiencies in the molecular assembly process that might be further exploited in identifying other glycosylated-amphiphiles that behave as low molecular weight hydrogelators.

Author contributions

Y. C. W.: investigation, formal analysis, methodology, visualization; writing – original draft; L. L. K.: conceptualization, investigation, visualization, writing – original draft; D. S. K.: investigation, methodology, writing – review & editing; B. S. D.: visualization, methodology, writing – review & editing; A. A.: supervision, writing – review & editing; M. K.: supervision, resources, writing – review & editing; J. E. P.: conceptualization, data curation, funding acquisition, supervision, writing – review & editing.

Conflicts of interest

J. E. P. has equity ownership in GlycoSurf, Inc. that is developing products related to the research being reported. The terms of this arrangement have been reviewed and approved by the University of Arizona in accordance with its policy on objectivity in research.

Acknowledgements

The authors gratefully acknowledge support of this research through a grant award from the National Science Foundation (CHE-1954467).

Crystallographic data were collected through the SCrALS (Service Crystallography at the Advanced Light Source) program at Beamline 12.2.1 at the Advanced Light Source (ALS), Lawrence Berkeley National Laboratory. The Advanced Light Source, is a DOE Office of Science User Facility under contract no. DE-AC02-05CH11231.

The authors gratefully acknowledge useful discussions with Drs. Robin Polt and Lajos Z. Szabó about synthetic aspects of this work.

References

1 X. Du, J. Zhou, J. Shi and B. Xu, *Chem. Rev.*, 2015, **115**, 13165–13307.
2 A. R. Hirst, B. Escuder, J. F. Miravet and D. K. Smith, *Angew. Chem., Int. Ed.*, 2008, **47**, 8002–8018.
3 E. R. Draper and D. J. Adams, *Chem*, 2017, **3**, 390–410.
4 L. A. Estroff and A. D. Hamilton, *Chem. Rev.*, 2004, **104**, 1201–1217.
5 M. De Loos, B. L. Feringa and J. H. Van Esch, *Eur. J. Org. Chem.*, 2005, 3615–3631.
6 N. M. Sangeetha and U. Maitra, *Chem. Soc. Rev.*, 2005, **34**, 821–836.
7 S. Ma, B. Yu, X. Pei and F. Zhou, *Polymer*, 2016, **98**, 516–535.
8 Y. Zhang, Z. Yang, F. Yuan, H. Gu, P. Gao and B. Xu, *J. Am. Chem. Soc.*, 2004, **126**, 15028–15029.
9 L. M. De Leon Rodriguez, Y. Hemar, J. Cornish and M. A. Brimble, *Chem. Soc. Rev.*, 2016, **45**, 4797–4824.
10 A. Kousar and C. Feng, *MethodsX*, 2019, **6**, 417–423.
11 A. E. Way, A. B. Korpusik, T. B. Dorsey, L. E. Buerkle, H. A. von Recum and S. J. Rowan, *Macromolecules*, 2014, **47**, 1810–1818.
12 M. Salim, H. Minamikawa, A. Sugimura and R. Hashim, *Med. Chem. Commun.*, 2014, **5**, 1602–1618.
13 L. Latxague, A. Gaubert and P. Barthélémy, *Molecules*, 2018, **23**, 1–25.
14 J. Fitremann, B. Lonetti, E. Fratini, I. Fabing, B. Payré, C. Boulé, I. Loubinoux, L. Vaysse and L. Oriol, *J. Colloid Interface Sci.*, 2017, **504**, 721–730.
15 L. Latxague, M. A. Ramin, A. Appavoo, P. Berto, M. Maisani, C. Ehret, O. Chassande and P. Barthélémy, *Angew. Chem., Int. Ed.*, 2015, **54**, 4517–4521.
16 M. Ikeda, R. Ochi, A. Wada and I. Hamachi, *Chem. Sci.*, 2010, **1**, 491–498.
17 N. Kimizuka and T. Nakashima, *Langmuir*, 2001, **17**, 6759–6761.
18 M. Bielejewski, K. Nowicka, N. Bielejewska and J. Tritt-Goc, *J. Electrochem. Soc.*, 2016, **163**, G187–G195.
19 A. Hemamalini and T. Mohan Das, *New J. Chem.*, 2013, **37**, 2419–2425.
20 S. R. Jadhav, P. K. Vemula, R. Kumar, S. R. Raghavan and G. John, *Angew. Chem., Int. Ed.*, 2010, **49**, 7695–7698.
21 S. Yamamichi, Y. Jinno, N. Haraya, T. Oyoshi, H. Tomitori, K. Kashiwagi and M. Yamanaka, *Chem. Commun.*, 2011, **47**, 10344–10346.
22 A. Vidyasagar, K. Handore and K. M. Sureshan, *Angew. Chem.*, 2011, **123**, 8171–8174.
23 J. H. Jung, J. A. Rim, W. S. Han, S. J. Lee, Y. J. Lee, E. J. Cho, J. S. Kim, Q. Ji and T. Shimizu, *Org. Biomol. Chem.*, 2006, **4**, 2033–2038.
24 G. Wang, S. Cheuk, K. Williams, V. Sharma, L. Dakessian and Z. Thorton, *Carbohydr. Res.*, 2006, **341**, 705–716.
25 G. Wang, S. Cheuk, H. Yang, N. Goyal, P. V. N. Reddy and B. Hopkinson, *Langmuir*, 2009, **25**, 8696–8705.
26 N. Goyal, S. Cheuk and G. Wang, *Tetrahedron*, 2010, **66**, 5962–5971.
27 J. Cui, J. Zheng, W. Qiao and X. Wan, *J. Colloid Interface Sci.*, 2008, **326**, 267–274.
28 L. E. Buerkle, R. Galleguillos and S. J. Rowan, *Soft Matter*, 2011, **7**, 6984–6990.
29 S. Nandi, H. J. Altenbach, B. Jakob, K. Lange, R. Ihizane, M. P. Schneider, Ü. Gün and A. Mayer, *Org. Lett.*, 2012, **14**, 3826–3829.
30 C. J. Capicciotti, M. Leclère, F. A. Perras, D. L. Bryce, H. Paulin, J. Harden, Y. Liu and R. N. Ben, *Chem. Sci.*, 2012, **3**, 1408–1416.
31 O. Gronwald and S. Shinkai, *Chem. – Eur. J.*, 2001, **7**, 4329–4334.
32 A. Brito, S. Kassem, R. L. Reis, R. V. Ulijn, R. A. Pires and I. Pashkuleva, *Chem*, 2021, **7**, 2943–2964.
33 N. Amanokura, K. Yoza, H. Shinmori, S. Shinkai and D. N. Reinhoudt, *J. Chem. Soc., Perkins Trans. 2*, 1998, 2585–2591.
34 P. Sakya, J. M. Seddon and V. Vill, *Liq. Cryst.*, 1997, **23**, 409–424.
35 H. D. Dhruv, M. A. Draper and D. W. Britt, *Chem. Mater.*, 2005, **17**, 6239–6245.
36 M. J. Clemente, J. Fitremann, M. Mauzac, J. L. Serrano and L. Oriol, *Langmuir*, 2011, **27**, 15236–15247.
37 M. J. Clemente, R. M. Tejedor, P. Romero, J. Fitremann and L. Oriol, *RSC Adv.*, 2012, **2**, 11419–11431.
38 K. Ide, T. Sato, J. Aoi, H. Do, K. Kobayashi, Y. Honda and K. Kirimura, *Chem. Lett.*, 2013, **42**, 657–659.
39 M. Mathiselvam, D. Loganathan and B. Varghese, *RSC Adv.*, 2013, **3**, 14528–14542.
40 J. H. Jung, S. Shinkai and T. Shimizu, *Chem. – Eur. J.*, 2002, **8**, 2684–2690.
41 P. Rajamalli, P. S. Sheet and E. Prasad, *Chem. Commun.*, 2013, **49**, 6758–6760.
42 J. Li, K. Fan, L. Niu, Y. Li and J. Song, *J. Phys. Chem. B*, 2013, **117**, 5989–5995.
43 N. Yan, Z. Xu, K. K. Diehn, S. R. Raghavan, Y. Fang and R. G. Weiss, *Langmuir*, 2013, **29**, 793–805.
44 K. P. C. Sekhar, H. Adicherla and R. R. Nayak, *Langmuir*, 2018, **34**, 8875–8886.
45 M. J. Clemente, P. Romero, J. L. Serrano, J. Fitremann and L. Oriol, *Chem. Mater.*, 2012, **24**, 3847–3858.
46 S. Akama, T. Maki and M. Yamanaka, *Chem. Commun.*, 2018, **54**, 8814–8817.
47 T. Maki, R. Yoshisaki, S. Akama and M. Yamanaka, *Polym. J.*, 2020, **52**, 931–938.
48 R. Yoshisaki, S. Kimura, M. Yokoya and M. Yamanaka, *Chem. – Asian J.*, 2021, **16**, 1937–1941.
49 L. L. Kegel, Y.-C. Wang, L. Szabo, R. Rolt and J. E. Pemberton, *Langmuir*, 2021, submitted.
50 H. A. van Doren, R. van der Geest, R. M. Kellogg and H. Wynberg, *Carbohydr. Res.*, 1989, **194**, 71–77.
51 J. R. Moffat and D. K. Smith, *Chem. Commun.*, 2008, 2248–2250.
52 G. A. Jeffrey and L. M. Wingert, *Liq. Cryst.*, 1992, **12**, 179–202.
53 H. Prade, R. Miethchene and V. Vill, *J. Prak. Chem.*, 1995, **337**, 427–440.

54 M. Guvendiren and J. A. Burdick, *Biomaterials*, 2010, **31**, 6511–6518.
55 T. H. Kim, D. B. An, S. H. Oh, M. K. Kang, H. H. Song and J. H. Lee, *Biomaterials*, 2015, **40**, 51–60.
56 S. Nemir, H. N. Hayenga and J. L. West, *Biotechnol. Bioeng.*, 2010, **105**, 636–644.
57 G. Liu, Z. Liu, N. Li, X. Wang, F. Zhou and W. Liu, *ACS Appl. Mater. Interfaces*, 2014, **6**, 20452–20463.
58 S. Ma, M. Scaraggi, D. Wang, X. Wang, Y. Liang, W. Liu, D. Dini and F. Zhou, *Adv. Funct. Mater.*, 2015, **25**, 7366–7374.
59 N. Bassik, B. T. Abebe, K. E. Laflin and D. H. Gracias, *Polymer*, 2010, **51**, 6093–6098.
60 P. D. Topham, J. R. Howse, C. J. Crook, S. P. Armes, R. A. L. Jones and A. J. Ryan, *Macromolecules*, 2007, **40**, 4393–4395.
61 K. Xu, J. Wang, S. Xiang, Q. Chen, Y. Yue, X. Su, C. Song and P. Wang, *Compos. Sci. Technol.*, 2007, **67**, 3480–3486.
62 X.-W. Peng, L.-X. Zhong, J.-L. Ren and R.-C. Sun, *J. Agric. Food Chem.*, 2012, **60**, 3909–3916.
63 B. Ni, M. Liu, S. Lü, L. Xie and Y. Wang, *J. Agric. Food. Chem.*, 2011, **59**, 10169–10175.
64 L. Z. Szabó, D. J. Hanrahan, E. M. Jones, E. Martin, J. E. Pemberton and R. Polt, *Carbohydr. Res.*, 2016, **422**, 1–4.
65 O. V. Dolomanov, L. J. Bourhis, R. J. Gildea, J. A. K. Howard and H. Puschmann, *J. Appl. Cryst.*, 2009, **42**, 339–341.
66 G. M. Sheldrick, *Acta Crystallogr.*, 2015, **A71**, 3–8.
67 G. M. Sheldrick, *Acta Crystallogr.*, 2015, **C71**, 3–8.
68 D. J. Adams, K. Morris, L. Chen, L. C. Serpell, J. Bacsa and G. M. Day, *Soft Matter*, 2010, **6**, 4144–4156.
69 K. A. Houton, K. L. Morris, L. Chen, M. Schmidtmann, J. T. A. Jones, L. C. Serpell, G. O. Lloyd and D. J. Adams, *Langmuir*, 2012, **28**, 9797–9806.
70 I. R. Sasselli, P. J. Halling, R. V. Ulijn and T. Tuttle, *ACS Nano*, 2016, **10**, 2661–2688.
71 Y. Wang, L. Tang and J. Yu, *Cryst. Growth Des.*, 2008, **8**, 884–889.
72 P. Zhu, X. Yan, Y. Su, Y. Yang and J. Li, *Chem. – Eur. J.*, 2010, **16**, 3176–3183.
73 B. Roy, P. Bairi and A. K. Nandi, *Soft Matter*, 2012, **8**, 2366–2369.
74 E. Radvar and H. S. Azevedo, *Macromol. Biosci.*, 2019, **19**, 1800221.
75 C. Peyrot, P. Lafite, L. Lemiègre and R. Daniellou, in *Carbohydrate Chemistry: Chemical and Biological Approaches*, ed. A. P. Rauter, T. Lindhorst and Y. Queneau, Royal Society of Chemistry, London, 2017, vol. 43, pp. 245–265.
76 G. Wang, N. Goyal, H. P. R. Mangunuru, H. Yang, S. Cheuk and P. V. N. Reddy, *J. Org. Chem.*, 2015, **80**, 733–743.
77 H. P. R. Mangunuru, J. R. Yerabolu, D. Liu and G. Wang, *Tetrahedron Lett.*, 2015, **56**, 82–85.
78 K. P. C. Sekhar, D. K. Swain, S. A. Holey, S. Bojja and R. R. Nayak, *Langmuir*, 2020, **36**, 3080–3088.
79 J. Mewis and N. J. Wagner, *Adv. Colloid Interface Sci.*, 2009, **147-148**, 214–227.
80 J. Chen, H. Park and K. Park, *J. Biomed. Mater. Res.*, 1999, **44**, 53–62.
81 V. Vill, T. Bocker, J. Thiem and F. Fischer, *Liq. Cryst.*, 1989, **6**, 349–356.
82 H. A. van Doren and L. M. Wingert, *Mol. Cryst. Liq. Cryst.*, 1991, **198**, 381–391.
83 H. M. von Minden, K. Brandenburg, U. Seydel, M. H. J. Koch, V. Garamus, R. Willumeit and V. Vill, *Chem. Phys. Lipids*, 2000, **106**, 157–179.
84 C. Fong, T. Le and C. J. Drummond, *Chem. Soc. Rev.*, 2012, **41**, 1297–1322.
85 K. K. Karukstis, W. C. Duim, G. R. Van Hecke and N. Hara, *J. Phys. Chem. B*, 2012, **116**, 3816–3822.
86 D. C. Carter, J. R. Ruble and G. A. Jeffrey, *Carbohydr. Res.*, 1982, **102**, 59–67.
87 G. A. Jeffrey and Y. Yeon, *Carbohydr. Res.*, 1992, **237**, 45–55.
88 H. V. Koningsveld, J. C. Jansen and A. J. J. Straathof, *Acta Crystallogr., Sect. C: Cryst. Struct. Commun.*, 1988, **C44**, 1054–1057.
89 G. A. Jeffrey, Y. Yeon and J. Abola, *Carbohydr. Res.*, 1987, **169**, 1–11.
90 S. Bhattacharjee and G. A. Jeffrey, *Mol. Cryst. Liq. Cryst.*, 1983, **101**, 247–260.